Construction and Building Materials 224 (2019) 863–879

Contents lists available at ScienceDirect

Construction and Building Materials

journal homepage: www.elsevier.com/locate/conbuildmat

Characterisation of polymer cement mortar composites containing carbon fibre or auxetic fabric overlays and inserts under flexure

Mohammad Asad, Manicka Dhanasekar *, Tatheer Zahra, David Thambiratnam

Queensland University of Technology, Brisbane, QLD 4000, Australia

HIGHLIGHTS

- Polymer cement matrix (PCM) with and without fabric overlays/inserts characterised.
- Benefits of carbon fibre (CF) and auxetic fabrics (AF) to PCM investigated.
- CF overlayed/inserted specimens exhibited debonding and high peak load.
- AF overlayed/inserted specimens exhibited no debonding and high energy absorption.
- An elastic FE with contact nonlinearity predicted debonding in CF but not in AF.

ARTICLE INFO

Article history:
Received 1 November 2018
Received in revised form 10 July 2019
Accepted 15 July 2019

Keywords:
Polymer cement matrix
Carbon fibre
Auxetic fabric
Debonding
Energy dissipation
Masonry

ABSTRACT

An experimental investigation on the flexural response of polymer cement mortar matrix overlayed or inserted with carbon fibre or auxetic fabric layers subject to four levels of rates of loading (1–150 mm/min) is reported. Seventy-two specimens made from plain polymer cement mortar, composites with auxetic and carbon fibre fabric layers overlayed at the bottom and inserted at the mid-depth of the specimens were prepared and tested under four point bending. The failure mode including debonding, peak load, load-deflection behaviour, longitudinal strain at peak load, ultimate stage and energy dissipation are reported. All composite specimens exhibited higher peak load, longitudinal strain and energy dissipation in comparison to the plain polymer mortar specimens. Auxetic fabric composites exhibited increased energy dissipation and longitudinal strain at peak load without any sign of debonding. Carbon fibre composites, on the other hand, failed due to debonding at a lower longitudinal strain. A finite element model is presented to demonstrate the debonding tendencies observed in the experiments. Increase in rate of loading improved the performance of the auxetic fabric composites but reduced the energy dissipation of carbon fibre composites.

1. Introduction

Cementitious renders are commonly used to improve durability or fire resistance of structures. In some instances, such as mortarless masonry structural walls, these renders are also required to resist lateral loading. In either case, where the render is impacted by flying debris during cyclonic events, blasts or other disasters, its energy absorption property becomes a key parameter in protecting the underlying structure. Carbon Fibre (CF) fabric [1–3] is used widely in structural rehabilitation applications. CF fabrics typically exhibit very high tensile strength (in the order of ~3000 MPa to ~4000 MPa), low density and high stiffness [4–6]; however, CF fabrics are shown vulnerable to delamination or debonding in [7–9], a phenomenon usually observed in low energy impact and blast loading events [10].

Auxetic fabric (AF) [11–15] is used in applications requiring high energy absorption such as crashworthiness of road vehicles [14,15] and fall-protection in biomedical engineering [14]; their application in civil engineering is new [4,13,16–20]. AF fabrics exhibit negative Poisson's ratio [21,22] and hence is expected to resist delamination [7,23,24] better than the CF as illustrated in Fig. 1.

Fig. 1 shows that the interfaces between the common engineering materials (such as CF and mortar matrix) are vulnerable to damage (delamination or overclosure) whilst the interfaces between AF and a common engineering material (such as mortar matrix) do not exhibit such vulnerabilities regardless of whether the composite is subject to tension or compression. This qualitative description is

* Corresponding author at: Queensland University of Technology, 2, George Street, Brisbane, QLD 4000, Australia.
E-mail address: m.dhanasekar@qut.edu.au (M. Dhanasekar).

https://doi.org/10.1016/j.conbuildmat.2019.07.120
0950-0618/

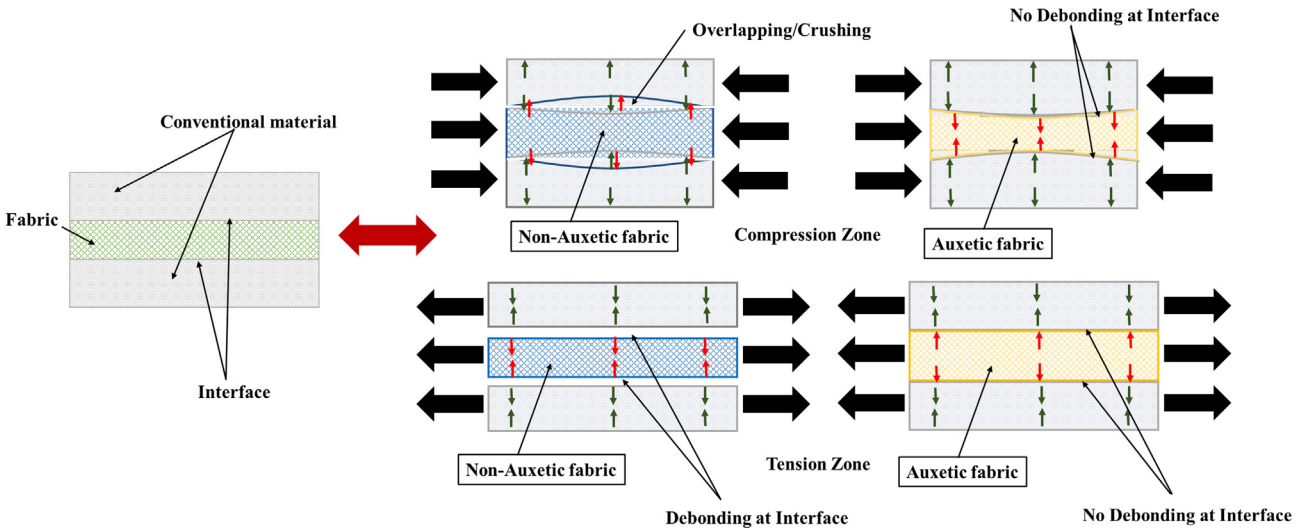

Fig. 1. Interface behaviour of Non-Auxetic (CF) and Auxetic Fabric (AF).

based on the zero-volume change (or positive Poisson's ratio) of the common engineering materials and the volume change (or negative Poisson's ratio) of the auxetic materials. To illustrate this phenomenon, an experimental investigation was carried out using specimens made from a polymer cement mortar composite containing CF or AF overlays or inserts subject to lateral loading.

This paper reports manufacturing of polymer cement composite specimens containing AF or CF overlays and inserts and testing them under bending. The overlays and inserts were positioned in the wet cementitious matrix without any aid of adhesive. Bond between these fabrics (AF or CF) and the matrix thus developed naturally through cement hydration products during curing. For better bond development, a commercially available polymer cement mix containing 2% polymer was chosen. Bending specimens were manufactured and tested under four distinct rates of loading and the response of the composites was measured using digital image correlation method. In total, seventy-two specimens were manufactured and tested. The AF composite specimens have shown superior performance than the CF composite specimens from the interfacial delamination and energy absorption perspectives.

This paper is structured as follows: Material properties, specimen preparation and test method used for AF and CF composite specimens are discussed in Section 2. Experimental results are discussed in Section 3. An elastic finite element method with contact nonlinearities is presented in Section 4 to illustrate the debonding potential at the CF and AF interfaces. Conclusions and recommendations for further research are presented in Section 5.

2. Experimental programme

Polymer cement matrix specimens of gross dimensions 240 mm long × 20 mm depth × 40 mm width were fabricated and tested. Single layer of AF or CF fabric was positioned either at the bottom (overlays) or at the mid-depth (inserts) of the specimen; some specimens were prepared with no such overlays or inserts as benchmark cases. After 14 days of air curing, the specimens were tested under four-point flexure at four different rates of deformation-controlled loading (1, 50, 100, 150 mm/min).

Digital Image Correlation (DIC) method was used to measure deformation and cracking in specimens. Failure modes, load-deflection curves, ultimate flexural stress and mean longitudinal strain for all specimens have been measured and are reported in this paper.

2.1. Properties of constituent materials

This section reports the properties of the three constituent materials: (1) polymer-cement matrix; (2) CF fabric and (3) AF fabric.

2.1.1. Polymer-cement matrix

Polymer-cement matrix was prepared using a commercially available mortar mix (2% polymer in Portland cement) satisfying the requirements of class R4 of the European standard EN1504-3 [25]. The pre-mixed mortar was blended with water in a proportion of 1:0.25 by weight. The mean compressive strength of the mortar matrix was determined by the authors as 6 MPa in [11]. This mix was previously used as thin layer mortar for concrete masonry structural walling by the authors; detailed information of this mix is specified in [11,26–28].

2.1.2. Auxetic fabric (AF)

The AF used in this research was made from a unidirectionally woven helical auxetic yarn of circular cross section; further details of weaving the fabric are reported in [29]. The nominal cross section area per unit width for the Auxetic fabric was 250 mm^2/m. The fabric was made in the UK and was tested under tension in a 1 kN INSTRON 5566 machine at QUT, Australia. The size and shape of the 1 mm thick auxetic fabric cut for testing are shown in Fig. 2.

Three specimens were tested under a uniform displacement rate of 1 mm/min, and the results were analysed using the DIC method. Maximum tensile strength of 50 MPa and negative poison's ratio (NPR) of −2.1 were obtained from the stress-strain plots of AF as in [24].

2.1.3. Carbon fibre (CF) fabric

CF fabrics are available with the fibres aligned unidirectional or bidirectional. Although bidirectional fabrics exhibit lower risk to debonding, in this research only the unidirectional CF fabric (shown in Fig. 3) was adopted to provide meaningful comparison with the AF (which was only available as a unidirectional fabric). A

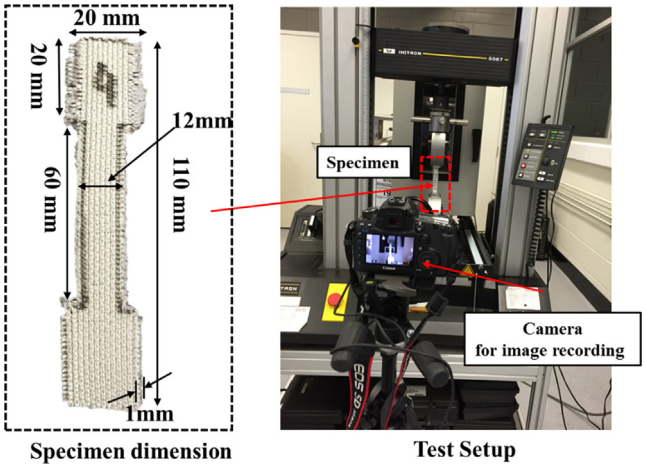

Fig. 2. Tensile testing of auxetic fabric.

plain-woven CF fabric is shown in Fig. 3(a). The average tensile strength and elastic modulus of the single-strand flax yarns extracted from the fabric were 3200 ± 300 MPa and 225 ± 50 GPa, respectively. The nominal cross-section area and strain to failure of the CF fabric provided by the supplier were 129 mm^2/m and 1.56% respectively.

2.2. Specimen preparation and strengthening technique

Seventy two (72) simply supported mortar specimens with and without AF/CF overlays under 4-point loading at different rates of displacement (1, 50, 100 and 150 mm/min) were tested. Fig. 4 shows the construction process of the specimens.

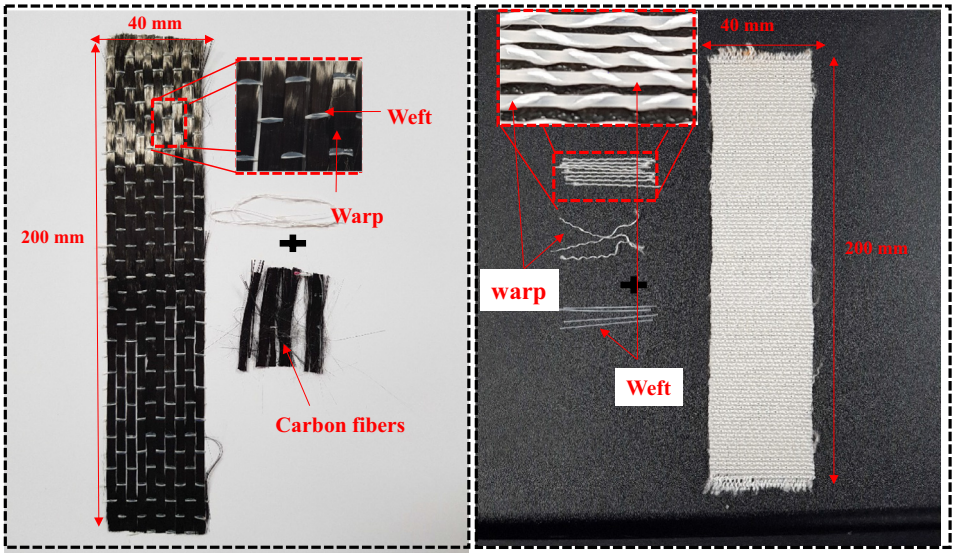

Fig. 3. Fabrics used.

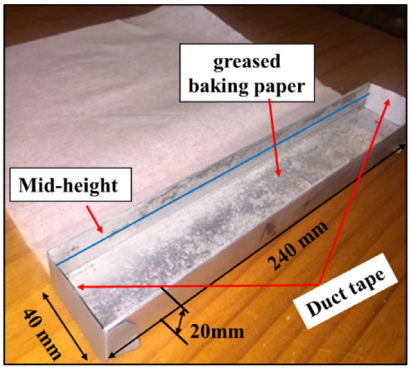

(a) Preparation of mould

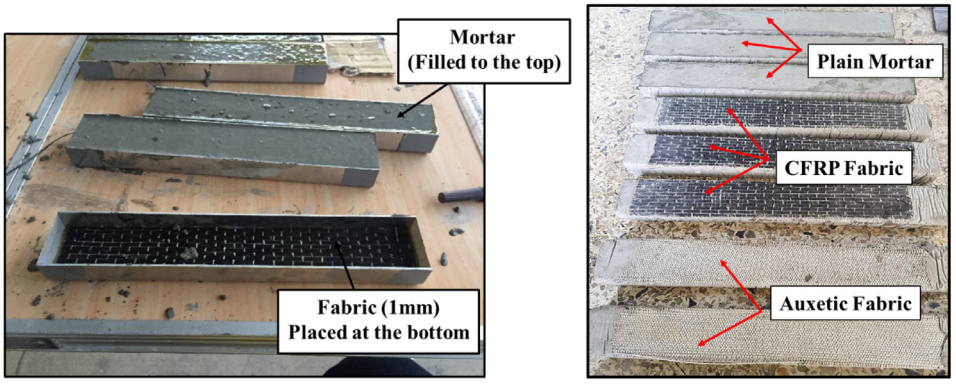

(b) Prepared specimens

Fig. 4. Specimen preparation procedure.

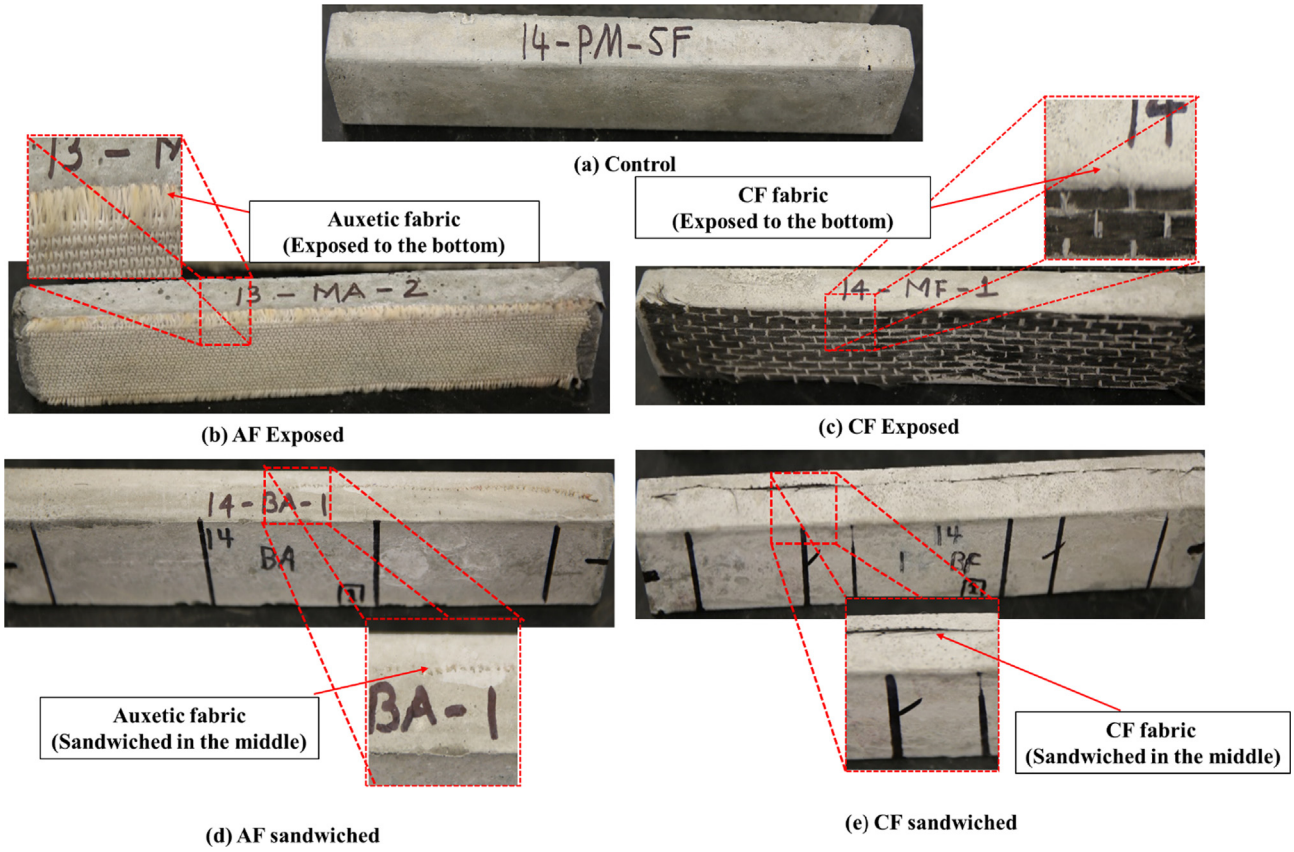

Fig. 5. Typical specimens prior to testing.

Rectangular C-shaped channel (240 mm long × 40 mm wide × 20 mm deep) moulds were used as formwork. The mould was initially capped at both ends with duct tape (Fig. 4(a)).

To enable easier de-moulding of the specimens, baking paper was placed inside the mould after greasing both sides of the paper as shown in Fig. 4(a). Mortar was mixed in a bowl and poured carefully on top of the baking paper. Where inserts were required, CF or AF fabric was placed on top of the baking paper (for overlay category specimens) prior to pouring mortar mix. For insert category specimens, mortar mix was poured to the level of a line drawn inside the mould indicating half-depth (Fig. 4a) before placing the AF or the CF fabric, and the mortar was then poured to the full depth of the mould. The specimens were removed from the mould after about 3 h of moulding and air cured, since air curing was shown better than moisture curing for the same mortar mix in thin layer mortar research [28,31–33]. Fig. 5 shows typical air cured specimens prior to testing.

Table 2 lists the identifier used for each specimen; the general identifier is AA-BB-CCC-D. The first two letters "AA" stand for type of specimen - plain mortar (PM)/ auxetic fabric (AF)/ carbon fibre (CF). The second two letters "BB" stand for location of insert – none (NO)/ inserted (SW)/ overlayed (EX). The third three letters "CCC" stand for rate of loading in mm/min – "001"/"050"/"100"/"150". The final single letter "D" stands for the specimen number in that particular group – "1"/"2"/"3"/"4" or "5"; note – a maximum of five specimens were fabricated in each group; some groups have had only three specimens.

2.3. Instrumentation and test setup

The specimens were tested under four-point bending using a 50 kN INSTRON 5569 machine with 0.00001 mm precision. Strain was measured using DIC system [27]; the test setup and the geometric details of the specimen are shown in Fig. 6.

Table 1
Average physical and mechanical properties of the Auxetic and CFRP fabric.

Properties	AF	CF [30]
Density	450 kg/m^3	1820 kg/m^3
Poisson's ratio	−2.17	0.23
Tensile modulus	400 MPa	225,000 MPa
Tensile strength	50 MPa	3500 MPa
Tensile strain	31.6%	1.56%

Table 2
Nomenclature and description of the developed specimens.

Specimen name	Explanation	Number of specimens
Group – I (CF and AF Composites at displacement rate of 1 mm/min)		
PM-NO-001-D	Plain Mortar	5
CF-EX-001-D	CF Overlays	5
AF-EX-001-D	AF Overlays	5
CF-SW-001-D	CF Inserts	3
AF-SW-001-D	AF Inserts	3
Group – II (CF and AF Composites at displacement rate of 50 mm/min)		
PM-NO-050-D	Plain Mortar	3
CF-EX-050-D	CF Overlays	3
AF-EX-050-D	AF Overlays	3
CF-SW-050-D	CF Inserts	3
AF-SW-050-D	AF Inserts	3
Group – III (CF and AF Composites at displacement rate of 100 mm/min)		
PM-NO-100-D	Plain Mortar	3
CF-EX-100-D	CF Overlays	3
AF-EX-100-D	AF Overlays	3
CF-SW-100-D	CF Inserts	3
AF-SW-100-D	AF Inserts	3
Group – IV (CF and AF Composites at displacement rate of 150 mm/min)		
PM-NO-150-D	Plain Mortar	5
CF-EX-150-D	CF Overlays	5
AF-EX-150-D	AF Overlays	5
CF-SW-150-D	CF Inserts	3
AF-SW-150-D	AF Inserts	3
Total number of tested samples		72

The flexural strength (modulus of rupture) of the mortar matrix was determined from the measured strain using the principles of linear strain distribution (plane section remains plane under flexure) in the basic structural mechanics [34]. The Young's modulus of elasticity was determined from the measured displacement of the specimen using the basic flexural displacement formula, ignoring shear deformation. The average tensile strength and the modulus of elasticity calculated from the four-point bending test on bare (containing no overlays or inserts) polymer-cement matrix specimens were 4.6 ± 2 MPa and 4.5 GPa respectively.

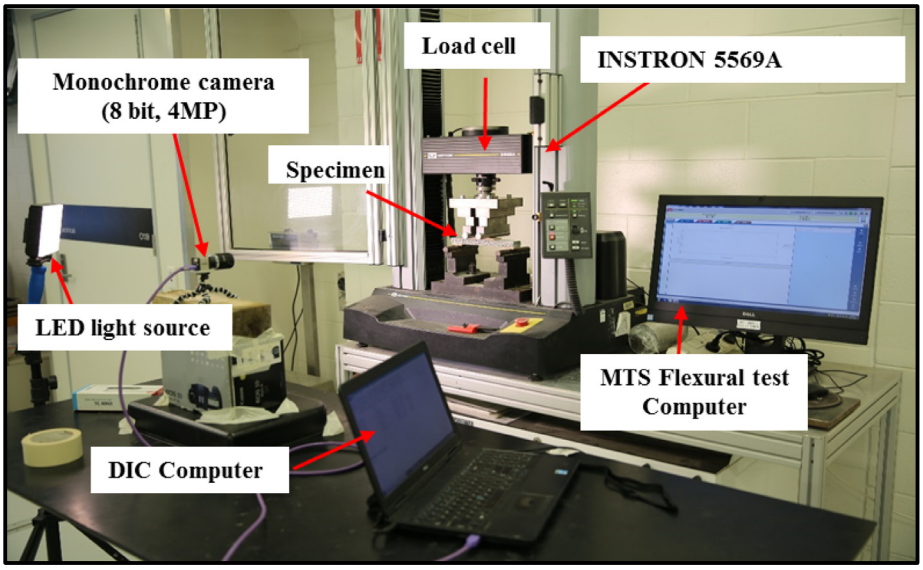

(a) Typical test setup

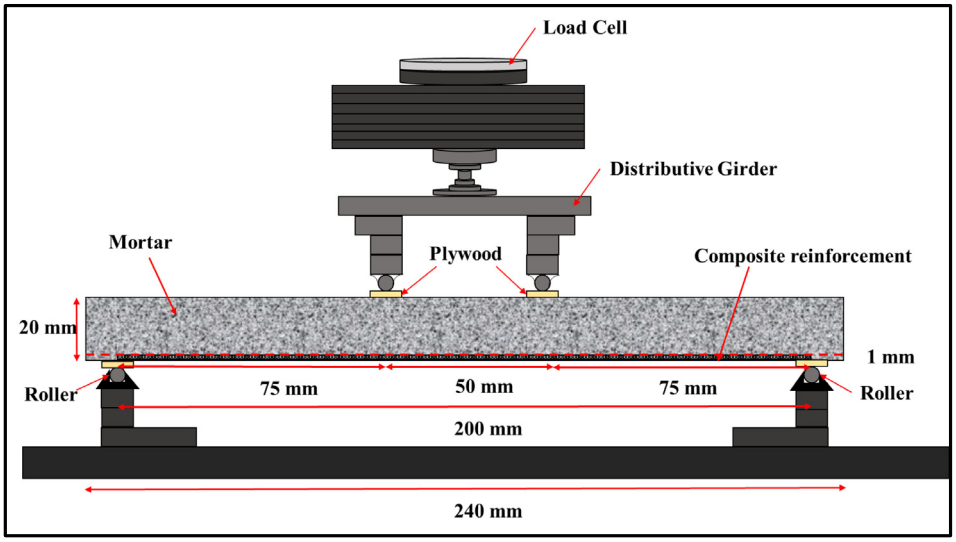

(b) Details of the specimen under testing

Fig. 6. Schematic view of the 4 point bending test.

A DIC system was used to measure the deformation of the region of interest (ROI) at the mid-span on the front face of the specimens. The DIC system comprised of an 8-bit 4-megapixel monochrome camera mounted on a small firm tripod and ISTRA 4D software from Dantec Dynamic [35,36]. The monochrome camera captured images at 161 frames per second (fps) for deflection rate 150 mm/min. The camera was positioned at the same height as the specimen and focused the front face of the specimen orthogonally. The ROI was speckled using a black marker for better contrast [37].

The system tracked the movement of pixels within a square facet of 27 × 27 pixels on each of the ROI image. The strain and deformation statistics (maximum, minimum and mean) were obtained from the DIC software for each facet.

The flexural load from the loading data were synchronised on the basis of clock time in the two computers. Stresses were computed using the load data acquired from the 50 kN INSTRON.

3. Experimental results and discussion

3.1. Failure modes using DIC

Fig. 7 shows a typical distribution of the longitudinal (flexural) strain plot as coloured fringes obtained from the DIC plot.

3.1.1. Plain mortar specimens containing NO inserts

Fig. 8 shows the view of the front surface of the plain mortar specimens. These specimens exhibited sudden failure following the formation of a single crack. Under very slow rate of loading (1 mm/min), the specimen exhibited failure at mid-span; whereas, under faster rates of loading (e.g., 150 mm/min), failure often occurred under one of the two loaded points. The ultimate load increased by 84% with the increase in loading rate of 149%.

3.1.2. Polymer cement mortar – CF composites

The colour fringes in Fig. 9 were obtained from the DIC analysis of longitudinal strain of the specimens containing CF overlays; at failure, the maximum tensile strain in the longitudinal direction was 0.13 (or 130,000 micro strain). Fig. 9 shows flexural cracking of the mortar matrix, fabric ruptures, and debonding that governed the failure modes of specimens containing CF inserts subject to lateral loading at the rate of 1 mm/min.

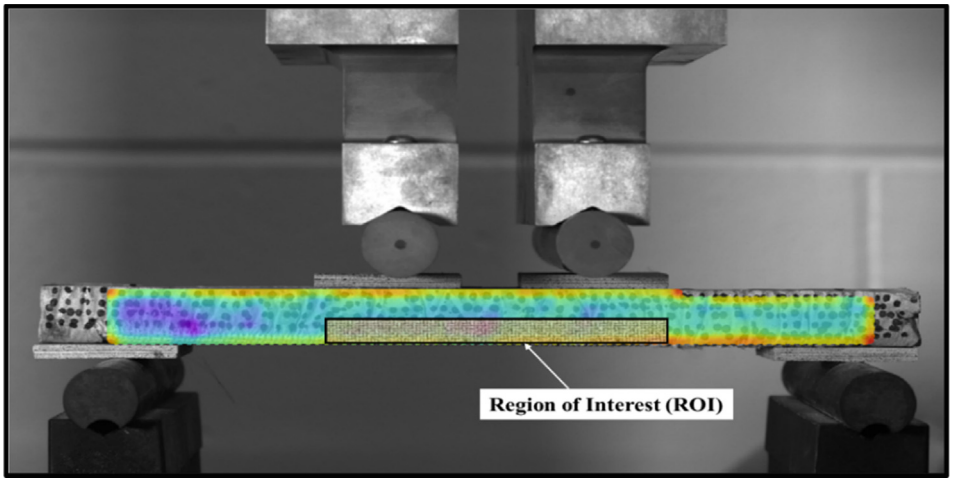

Fig. 7. A typical DIC plot of strain contour in the ROI.

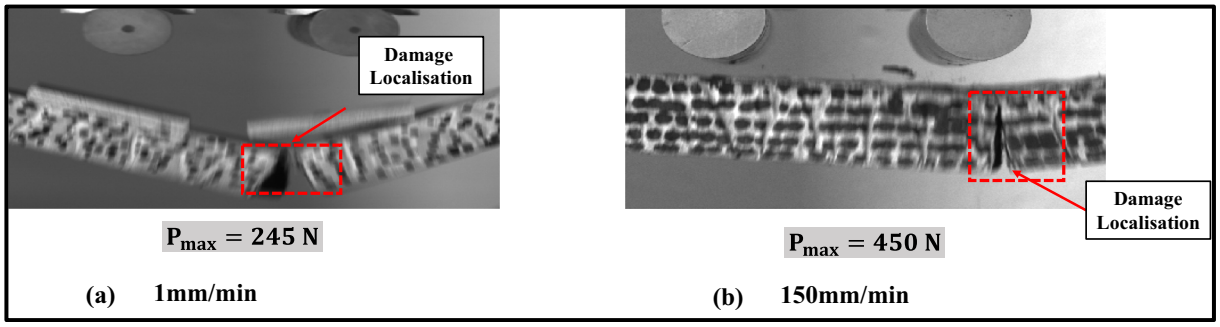

Fig. 8. Failure of the control specimens.

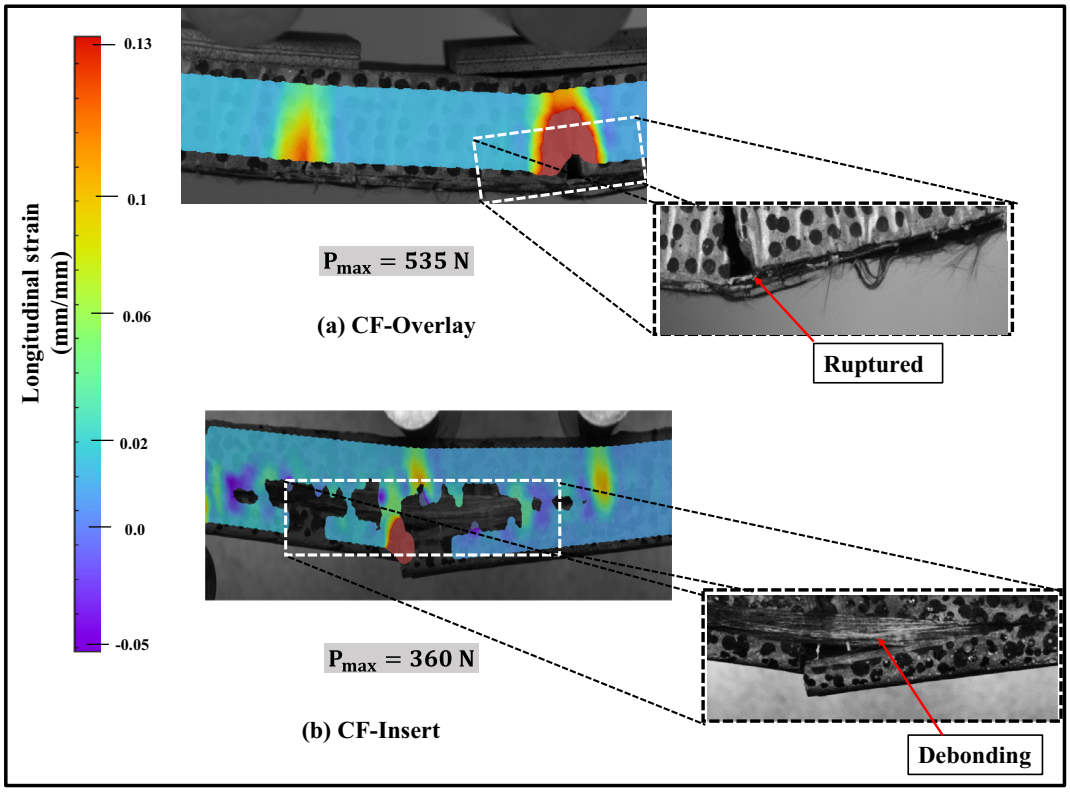

Fig. 9. Failure of mortar specimens containing CF specimens under 1 mm/min.

In the specimens containing CF fabrics (either overlay or insert), tensile cracks emanated from the location of tensile fabric and propagated towards the compression zone of the specimen. Essentially, the overlayed specimens responded better than the insert specimens at half-depth for which the peak load reduced by 49%. The load transfer mechanism continued till multiple diagonal tension cracks developed in the composite matrix. Ultimately, the specimen failed due to a widening of the dominant crack.

Higher rate of loading (e.g., 150 mm/min) did not affect the mode of failure as evident from Fig. 10. Cracking of the mortar matrix, delamination and fracturing of the CF layer are evident from Fig. 10 – irrespective of whether the inserts are at the bottom layer (overlayed) or at the mid-depth of the specimen (inserted).

Under faster rate of loading, the specimens failed exhibiting inclined cracks at one of the loaded points due to shear dominance. The overlayed composite render exhibited rupture of the fabric due to the bending/kinking failure of the specimen. The longitudinal strain shown in the colour fringes was determined from the DIC analysis; at failure, the maximum tensile strain in the longitudinal direction was 0.13 (or 130,000 micro strain) – which was similar to the failure of specimens under the lower (1 mm/min) rate of loading.

3.1.3. Polymer cement mortar – AF composites

Flexural failure modes of the overlayed and the inserted AF composites under 1 mm/min, and 150 mm/min loading are shown in Figs. 11 and 12 respectively.

The flexural cracks observed in the tension face of the overlayed composite specimen are similar to the specimens under 150 mm/min as shown in Fig. 12. The failure mode exhibits no debonding – which is contrary to the composites containing CF inserts. The negative Poisson's ratio appeared to have contributed to this desirable no-delamination failure mode consistent with the expected response discussed with reference to Fig. 1 in this paper.

Fig. 11 shows that the composite specimens exhibit flexural crack in the tensile zone with no evidence of debonding at the interface similar to those specimens under 1 mm/min loading. Under 150 mm/min, AF composite specimens exhibited higher strength in comparison to the AF composite specimens under 1 mm/min loading for both the overlayed and inserted cases. The beneficial effect of the negative Poisson's ratio is thus obvious.

The longitudinal strains corresponding to the ultimate load stage shown in Figs. 11 and 12 is 0.13 (130,000 microstrain) – which is similar to the longitudinal strain in the specimens containing CF inserts (Figs. 9 and 10). In spite of the same level of strain, it is noticeable that the AF inserts prevented delamination whilst the CF inserts could not.

The failure modes observed from the 72 specimens are schematically presented in Fig. 13. Failure modes are grouped for the PM, CF and AF specimens in this Fig. 13.

PM specimens failed due to formation of a single, wide crack either at mid span or near one of the loading points as shown in group I (Fig. 13). CF specimens exhibited multiple cracks but at failure either one of two cracks widened in association with debonding and fracturing of the fabric; such failures were common for both the overlayed and the inserted specimens (Group II, Fig. 13). The overlayed specimens also exhibited longitudinal shear slip. The AF specimens also failed similar to CF specimens but with no evidence of delamination and/ or fracturing of the fabric (Group III, Fig. 13). This beneficial response of the AF to the polymer cement matrix is a key finding of the research reported in this paper.

3.2. Load-displacement response

Typical load-deflection curves of the overlay specimens containing carbon fibre (CF) or auxetic fabric (AF) and the control specimen (plain mortar) are exhibited in Fig. 14. The corresponding failure mode of each of these specimens is also provided as an image insert in these figures.

Transition points (a), (b) and (c) marked on the load-displacement curves of these specimens in Fig. 14 are defined as below:

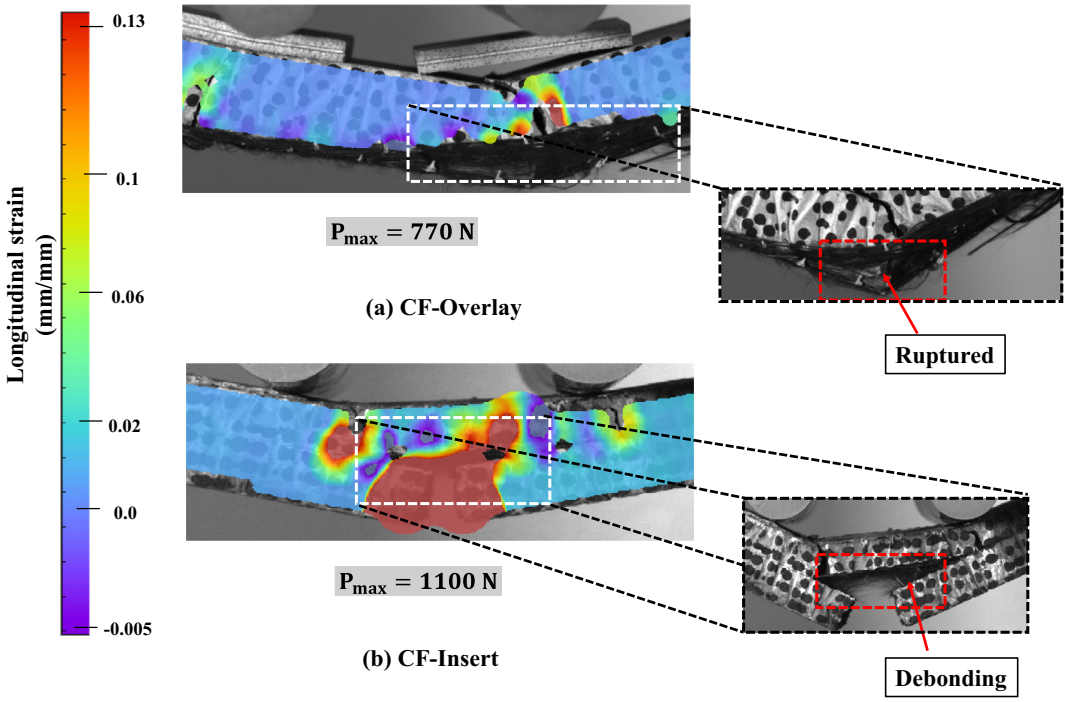

Fig. 10. Failure mode of specimens containing CF specimens at 150 mm/min.

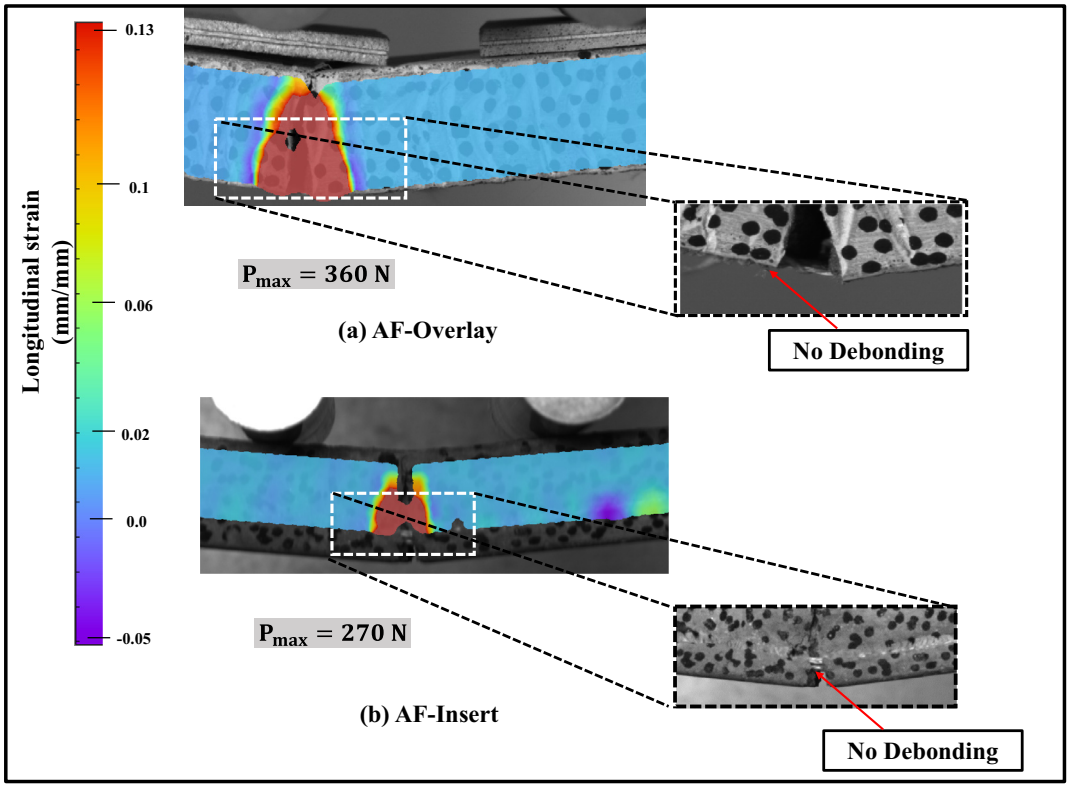

Fig. 11. Failure of specimens containing AF specimens under 1 mm/min loading.

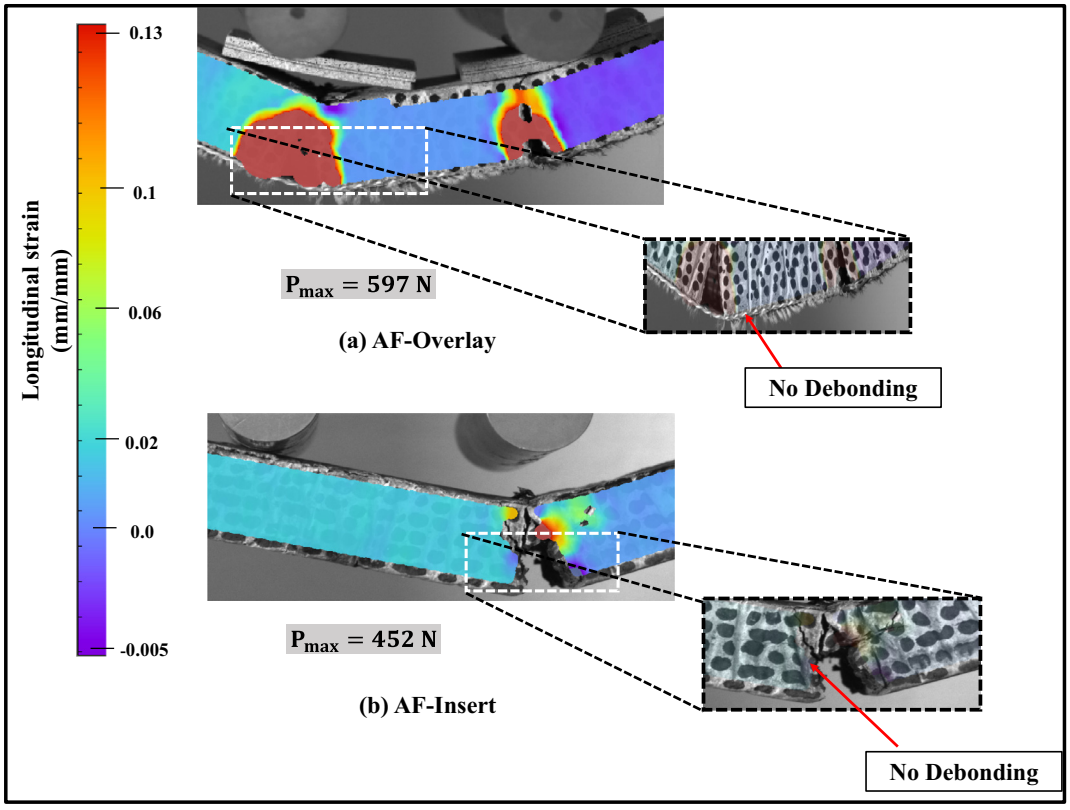

Fig. 12. Failure of specimens containing AF specimens under 150 mm/min.

Point (a) – Initiation of cracking: First crack occurred at a very low displacement corresponding to approximately 25% of peak load in all the specimens.

Point (b) – Peak load: All specimens showed steady increase in the load capacity after initial cracking until peak load was realised. The control specimen showed the lowest peak load of

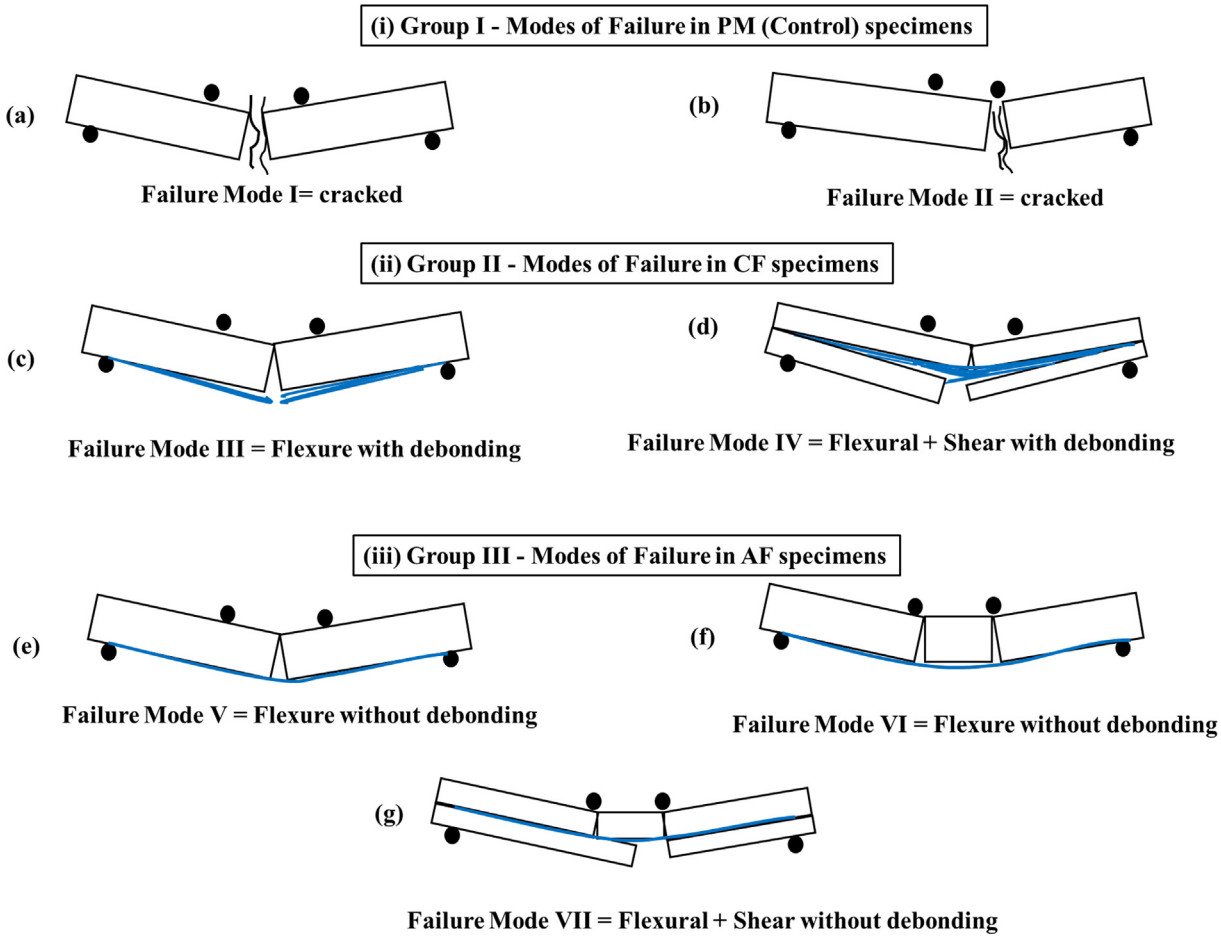

Fig. 13. Failure modes of the tested specimens.

around 300 kN; CF overlay specimen exhibited the largest load of about 570 kN, whilst the AF specimens peaked at 380 kN.
Point (c) – Ultimate point: The ultimate point is defined as the point where the mortar matrix fully damaged exhibiting clear localisation of damage with wider cracks in the tension zone and crushed mortar in the compression zone. The ultimate points of the CF and AF composites are identified when the damage was completely localised across the whole thickness of the mortar as marked in Fig. 14(a) and (b), respectively. At ultimate, the CF specimens exhibited high levels of debonding and in many instances fracture of CF fabric; none of the AF specimens, on the other hand, exhibited debonding or fracture of fabric at ultimate stage. As the load – displacement characteristics of the CF and AF composites shown in Fig. 14(a) and (b) respectively are significantly different, the displacements corresponding to these damage localisation states varied. The control specimen failed suddenly exhibiting brittle load-displacement plot in Fig. 14(c).

Both the CF and AF overlay specimens exhibited crack initiation at about 0.2 mm deflection (identified by point (a)). With further increase in the length of this first crack, both specimens exhibited true composite action exhibited by the strains in the mortar and the adjacent fabric; as the CF was stiffer than the AF, the stress in the CF fabric was larger than AF and hence the CF specimens exhibited larger peak load – however, both the CF and AF specimens exhibited peak load at around 0.6 mm deflection. In the post peak regime, the CF specimens exhibited onset and growth of delamination that culminated in substantial loss of load resistance leading to full damage localisation of the mortar matrix with little assistance from the delaminated CF fabric. At around 4 mm displacement, the CF specimen attained ultimate stage leading to rupture of the CF fabric. A loss of 80% of peak load provided sufficiently accurate definition of the ultimate state for the CF composite as identified on the load-displacement curve of the CF composite in Fig. 14(a).

In comparison, the AF specimens showed a sudden drop in the capacity immediately after peak load, reflecting the lower stiffness of the auxetic fabric; however, as debonding was not evident, these specimens regained load resistance and sustained about 67% of the peak load for a much larger increase in deflection until 13 mm deflection was achieved. This enhancement is mainly due to the fact that AF fabric remain fully bonded to the matrix, which is clearly evident in the snapshots of the specimen provided within Fig. 14(b). The ultimate state of the AF composite roughly coincided with its second peak stage as shown in Fig. 14(b).

Ultimate stage of brittle structures is usually considered corresponding to loss of 20% of peak load [38–40]. Although this significantly differs to the consideration of the ultimate stage of composites corresponding to 80% drop in peak load as reported in this section (which corresponded to the fracture of the CF) but is consistent with the definitions provided by Naaman and Jeong [41], where the rupture of tensile layers in brittle matrix is defined as the ultimate. Recently Hadi and Yuen [42] used the same definition for the ultimate stage of the glass fibre reinforced composite structures. Therefore, use of 80% drop in peak load as ultimate stage appears justifiable.

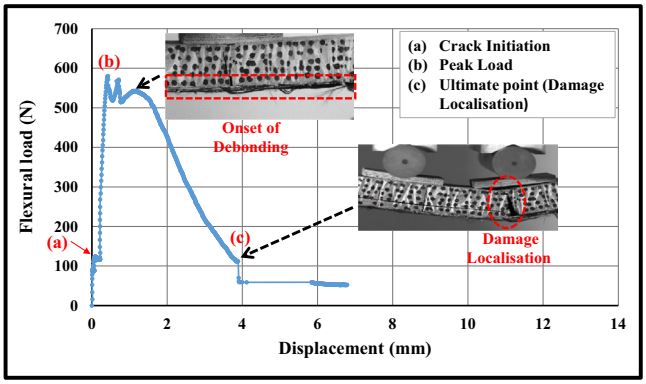

(a) CF overlay specimen

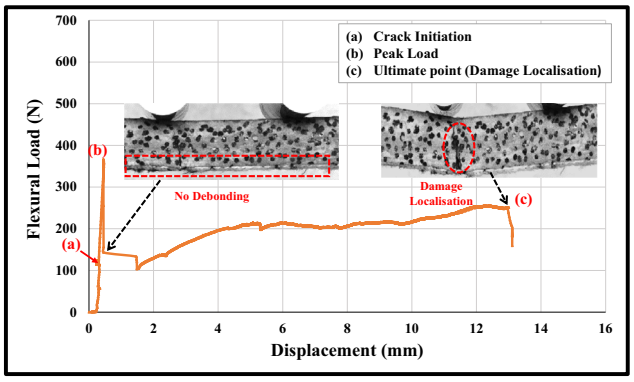

(b) AF overlay specimen

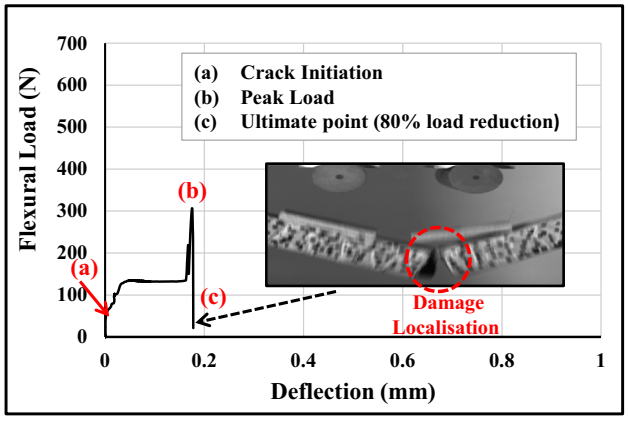

(c) Control specimen

Fig. 14. Deformation response of typical specimens.

3.3. Energy dissipation

Dissipated energy was determined from the area under the flexural load-displacement curve up to the ultimate point. As the load–displacement characteristics of the CF and AF composites shown in Fig. 14(a) and (b) respectively are significantly different, the displacements corresponding to these damage localisation states varied. To calculate the area, an image processing freeware ImageJ [43] was used. Calculation of the energy dissipation from the load-displacement curve is illustrated in Fig. 15.

Load-displacement curve of specimen AF-EX-001-5 was used as an illustration. For calibrating the dimensions in the software, grey scale XY plot with equal magnitudes for horizontal (X) and vertical (Y) axes was required; hence, the maximum displacement at X axis was set as 700 mm. Correspondingly, the X and Y axis lengths were divided equally to obtain a square box for the calibration.

The area under the curve was calculated by multiplying the points on the curve with their corresponding X and Y axis units. The summation of all the multiple of the individual points provided the total energy dissipation in the unit J (Joules). For the curve shown in Fig. 15, the dissipated energy is 7.25 J. Dissipated energy for all the specimen was determined using the same method and is listed in Table 3.

3.4. Delamination

Delamination of the overlays/inserts from the mortar matrix was determined from the analysis of the displacement field obtained from the DIC results as displayed in Fig. 16.

As the thickness of the overlays/inserts was very small, it was difficult to exactly select a facet (27 pixels × 27 pixels) covering only the overlay / insert when they delaminated. Therefore, delamination of the overlay from the matrix in the overlayed-type specimens could not be analysed using the ISTRA4D; the inserted-type specimens were, however, used in the analysis by selecting two facets on the mortar matrix above and below the insert (identified as points *a* and *b* in the Fig. 16, where the vertical displacement time series at the centre of each of these facets is plotted). The two traces of displacement time series (for points *a* and *b*) shown in Fig. 16(a) illustrate the interfacial debonding of the matrix layer below the CF insert. The traces in Fig. 16(b) on the other hand coexists, illustrating no such debonding in the AF specimen.

3.5. Longitudinal strain

The longitudinal strain corresponding to the ultimate load stage was measured at a point Q shown in Fig. 17 for the control, inserted and overlayed composite specimens using DIC. The point Q was located at mid-span 2 mm above the bottom surface layer. These measured longitudinal strains at Q for all the specimens are presented in Fig. 18; this plot provides an appreciation of the effect of the rate of loading (1, 50, 100 and 150 mm/min) to the type of specimens.

Fig. 18 shows that the AF composite specimens exhibit significant increase in the longitudinal strain (corresponding to the peak load) as compared to the control specimens. With the increase in the loading rate from 1 to 150 mm/min, all specimens containing AF overlays/inserts significant increase in the longitudinal strain. However, the overlayed specimens exhibited larger strain compared to their sandwich counterparts due to larger lever arm between the tensile forces in AF and the compression in the polymer mortar matrix.

On the contrary, the specimens containing CF overlays have exhibited reduction in longitudinal strain with the increase in the rate of loading, which is akin to the control specimens. This phenomenon of reduction in the longitudinal strain of the CF overlays and the control specimens with the increase in the rate of loading is a reflection of brittle failure. The CF specimens failed due to early debonding culminated in fabric rupture with the increase in the rate of deflection. Whereas, no sign of debonding was observed in the AF composite specimens due to the effective contribution of the negative Poisson's ratio of AF inserts.

AF specimens exhibited enhanced (up to 3.2 times) longitudinal strain in comparison to the respective CF overlayed composites at the peak load stage. Similarly, the AF inserted composite specimens, experienced enhanced longitudinal strain of 6 times compared to the CF inserted composite.

Overall, the performance of AF overlayed composites was better than all other forms considered. The AF overlayed configuration

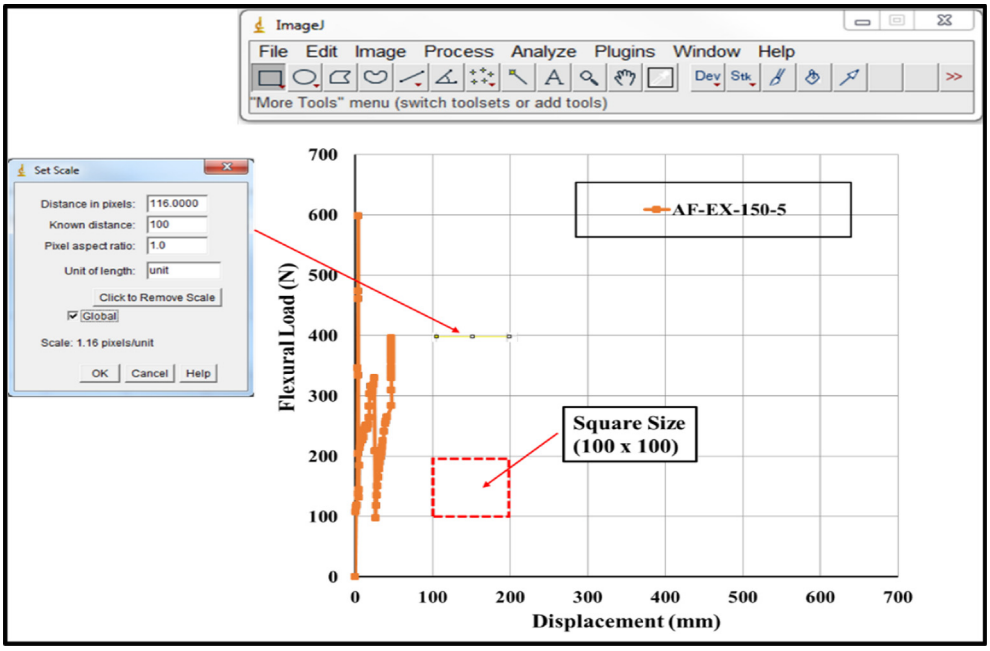

Fig. 15. Calculation of energy dissipation using ImageJ software.

Table 3
Summary of results for specimen groups.

Specimen group (1)	Rate of loading (mm/min) (2)	Mean peak load in N (CoV; %) (3)	Mean load (N) at ultimate point (4)	Mean deflection at peak load (mm) (5)	Dissipated energy (Avg.) J, (CoV; %) (6)	Failure shape (Refer: Fig. 13) (7)
PM-NO-001	1	310 (8.5)	10.7	0.012	0.064 (14.2)	(a)
CF-EX-001		450 (7.1)	44.1	0.95	1.56 (15.6)	(c)
AF-EX-001		350 (6.5)	243.4	1.10	1.53 (7.3)	(e)
CF-SW-001		360 (10.1)	51.1	0.78	1.13 (8.4)	(d)
AF-SW-001		270 (15.6)	153.5	1.09	1.09 (5.1)	(g)
PM-NO-050	50	360 (1.4)	12.2	0.017	0.031 (12.6)	(a),(b)
CF-EX-050		540 (8.3)	79.5	2.10	3.07 (14.3)	(c)
AF-EX-050		441 (8.9)	288.2	2.28	4.9 (3.7)	(e)
CF-SW-050		445 (13.3)	45.7	0.71	4.2 (17.7)	(d)
AF-SW-050		350 (17.5)	187.6	2.30	5.135 (21.1)	(g)
PM-NO-100	100	380 (6.7)	11.5	0.11	0.016 (13.2)	(b)
CF-EX-100		650 (10.7)	83.3	2.27	1.6 (21.9)	(c)
AF-EX-100		470 (10.8)	258.6	2.33	3.19 (24.5)	(e),(f)
CF-SW-100		600 (14.5)	56.0	1.30	4.74 (14.7)	(d)
AF-SW-100		340 (13.1)	196.3	2.20	6.28 (26.4)	(g)
PM-NO-150	150	450 (14.6)	15.1	0.13	0.13 (14.0)	(b)
CF-EX-150		770 (14.1)	133.2	2.21	2.66 (8.6)	(c)
AF-EX-150		540 (16.0)	325.7	3.03	4.79 (16.3)	(e),(f)
CF-SW-150		700 (15.4)	78.4	1.59	5.08 (12.9)	(c),(d)
AF-SW-150		450 (16.8)	217.2	2.69	6.55 (24.9)	(g)

enhanced the ductile behaviour at higher rates of loading, which may be interpreted that where renders of AF-polymer mortar composites are considered, these fabrics are better positioned at or close to the outer surface of the render.

3.6. Summary of test results and discussions

Table 3 provides summary of the test results for all the specimens.

Mean and coefficient of variation (CoV) of peak load for each group of specimens are displayed in column 3. Each group of specimens exhibited CoV values in a range from a low of 1.4% to a high of 17.5%. The CoV of the control mortar specimen (without any fabric) was at the lower band of the range. The variability increased to the higher band of the range in the CF composite because of the bond failures and rupture of the CF composites. The AF composites exhibited variability in a middle band of this range. Minor deviations on the actual position of the fabrics in the wet mortar composites could also have contributed to this variability in the CF and AF composites compared to the control mortar specimens without any fabrics.

Mean load at the ultimate point is shown in Column 4. The mean displacements corresponding to the peak loads is shown in column 5. Column 6 shows the dissipated energy with its coefficient of variance and column 7 refers to the observed mode of failure summarised in Fig. 13.

Table 3 shows that all specimens exhibited increase in peak load with the increase in rate of loading, which is consistent to the mechanism of failure of engineering materials. Specimens with AF overlays/inserts exhibited only marginal increase in peak load of approximately 12% at the lowest rate of loading to 20% at the highest rate of loading compared to the respective plain mortar specimens (refer to Column 3 of Table 3). However, the CF overlayed specimens, on the other hand, exhibited a significant

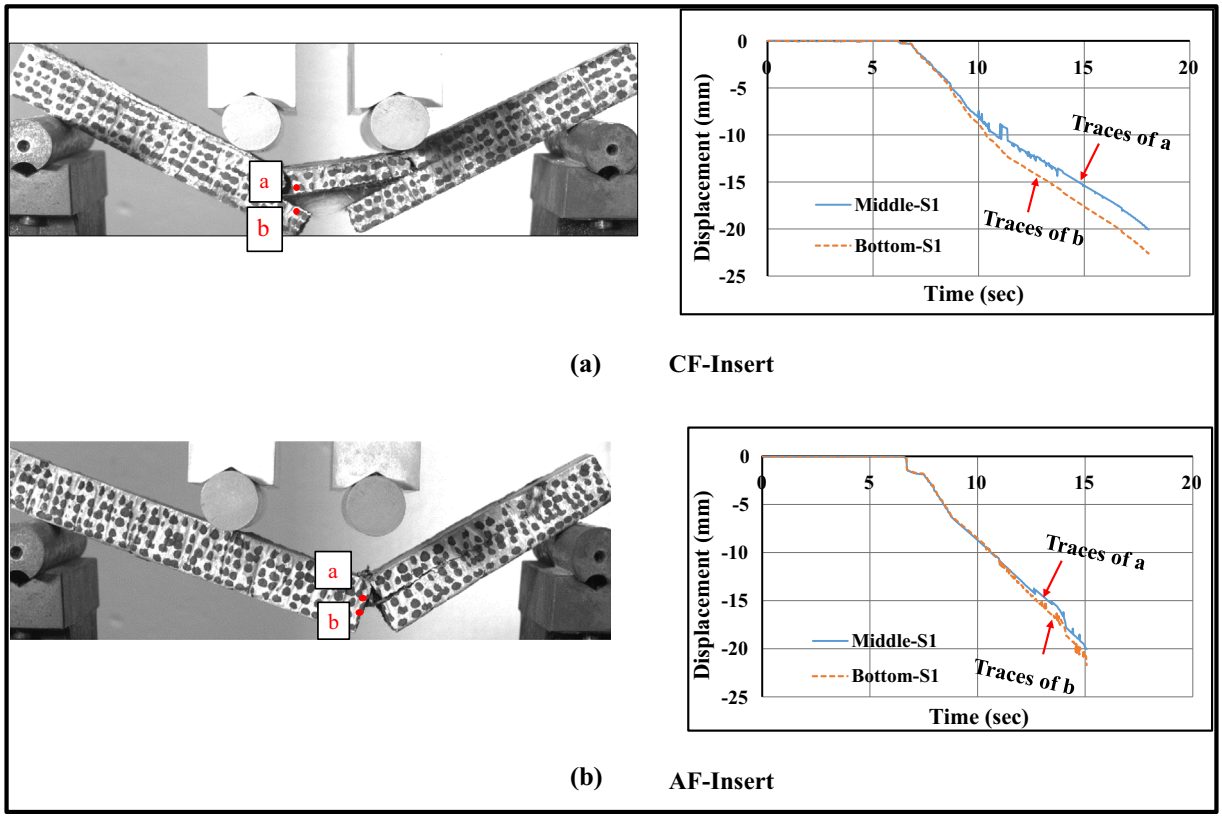

Fig. 16. Vertical displacement time series for CF and AF specimens.

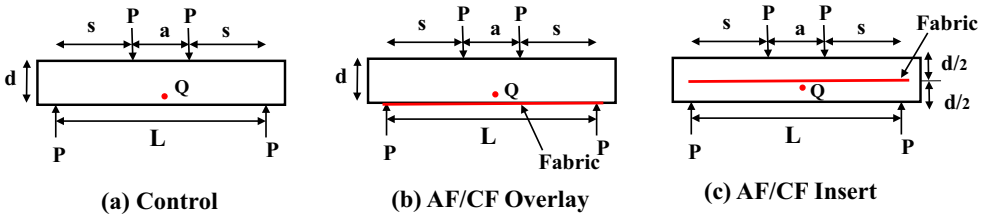

Fig. 17. Point of measurement for maximum longitudinal strain using DIC.

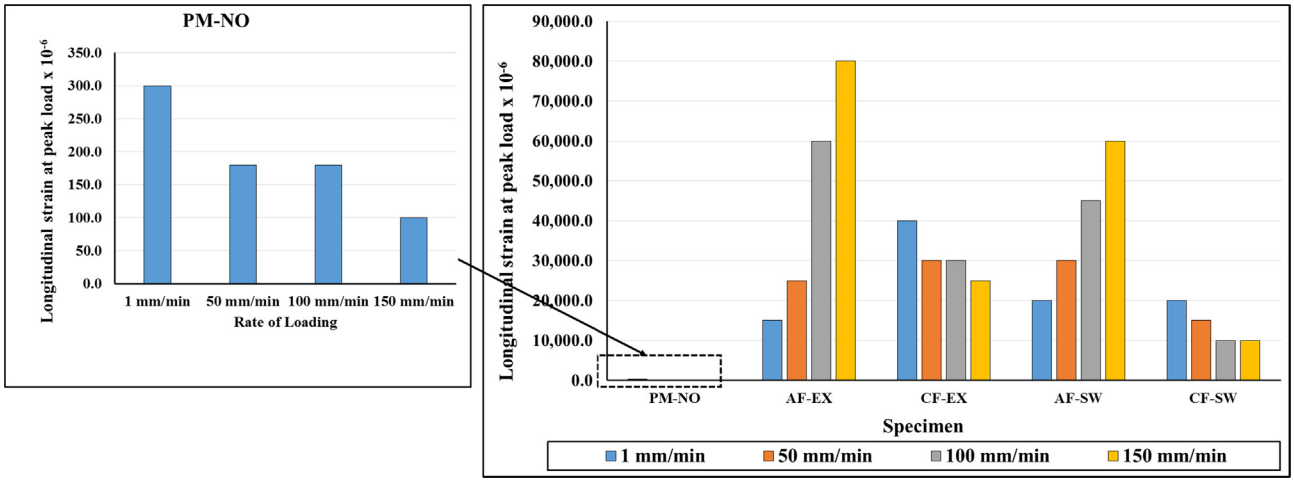

Fig. 18. Maximum longitudinal strain of specimens for different rate of deflection.

increase in peak load of approximately 45% at the lowest rate of loading to 71% at the highest rate of loading employed compared to the respective plain polymer mortar specimens.

Both the AF and the CF insert specimens exhibited lower peak load than the corresponding AF and CF overlayed specimens since the effective depth of these specimens is halved. It can be concluded from the column 3 (of Table 3) that the specimens with CF inserts can be more effective (in terms of peak load), even when their effective depth is halved. Whereas, it can be observed from Column 4 (of Table 3) that the overlay and insertion of AF layer resulted in significant enhancement of the post peak displacements and flexural load at the ultimate point. Hence, larger post peak displacements and the greater flexural load at ultimate point provide larger energy dissipation of the AF composite specimens compared to the CF composite specimens.

Table 3 (Column 6) also reveals that all controlled specimens dissipated very low energy in comparison with all other specimens. This illustrates any form of overlaying/inserting fabrics is better than not having any such overlay/insert. The AF overlayed specimens are the best performing group; their dissipated energy is larger than the corresponding controlled specimens by a factor of 134 under the loading rate of 1 mm/min and an enhanced factor of 160 under the loading rate of 150 mm/min. This phenomenon is consistent with the contribution of AF inserts towards sustaining larger post-peak displacements over a longer period of time. On the other hand, the CF overlayed specimens, at 150 mm/min, exhibited a lower energy dissipation by an amount of 25% in comparison to the AF overlayed specimens. This reduction in the magnitude of energy dissipation for the CF specimens is due to early debonding of the CF inserts at the interface (as shown in Fig. 14a).

4. Finite element model

With a view to demonstrating the different failure mechanisms exhibited by the CF and AF composites, an elastic 3D finite element model with contact only nonlinearity between the fabrics and matrix was established. In this model four noded shell elements (S4R) with reduced integration [44–46] were used to describe the geometry of the cementitious matrix and continuum shell element (SC8R) for the fabric; the interface between them was established using the interface modelling method with tension and shear separation capability described in [32,33]. This contact-only nonlinear elastic model was established in ABAQUS. The models contained 12036 DOF and were solved in SGI Altix XE clusters available at the high performance computing facility, Queensland University of Technology. The elastic modulus of mortar matrix was taken as 4000 MPa. Table 1 contains the properties of the CF and AF fabrics. The tension and shear stiffness and limit values used in the model were 250 N/mm^3, 1.81 MPa for CF fabric and 25 N/mm^3, 1.5 MPa for AF fabric respectively.

Fig. 19 shows the details of the mesh and boundary conditions adopted in the analysis; for brevity, convergence studies carried out in determining this mesh is not reported.

Monotonically increasing displacement was imposed up to 1.2 mm to illustrate the response of the interface – in particular the occurrence or otherwise of debonding in the CF and AF composites. Longitudinal strain at the bottom face of the mortar and the top face of CF/AF fabric was output for deflections from 0.04 to 1.2 mm in Figs. 20, and 21 respectively.

The numerical result of strain is compared with the average strain obtained from the experimental result for displacement of 0.04 mm in both CF and AF composite specimens. The longitudinal strain in mortar of the CF composite was 60 μm (experimental) – which compares favourably with the 65 μm (FE prediction). Similarly the longitudinal strain in mortar of the AF composite was 120 μm (experimental) – which compares favourably with the 130 μm (FE prediction). Given the variability in the experimental strains, these predictions are regarded close agreement with approximately 8% error. Due to lower stiffness of AF fabric, the mortar bending stress in the AF composite was larger than that of the CF composite.

As shown in Fig. 20, the longitudinal strain in the CF fabric remained larger than that of the mortar (as it should be) until the deflection increased to 0.7 mm, where the strain in the CF fab-

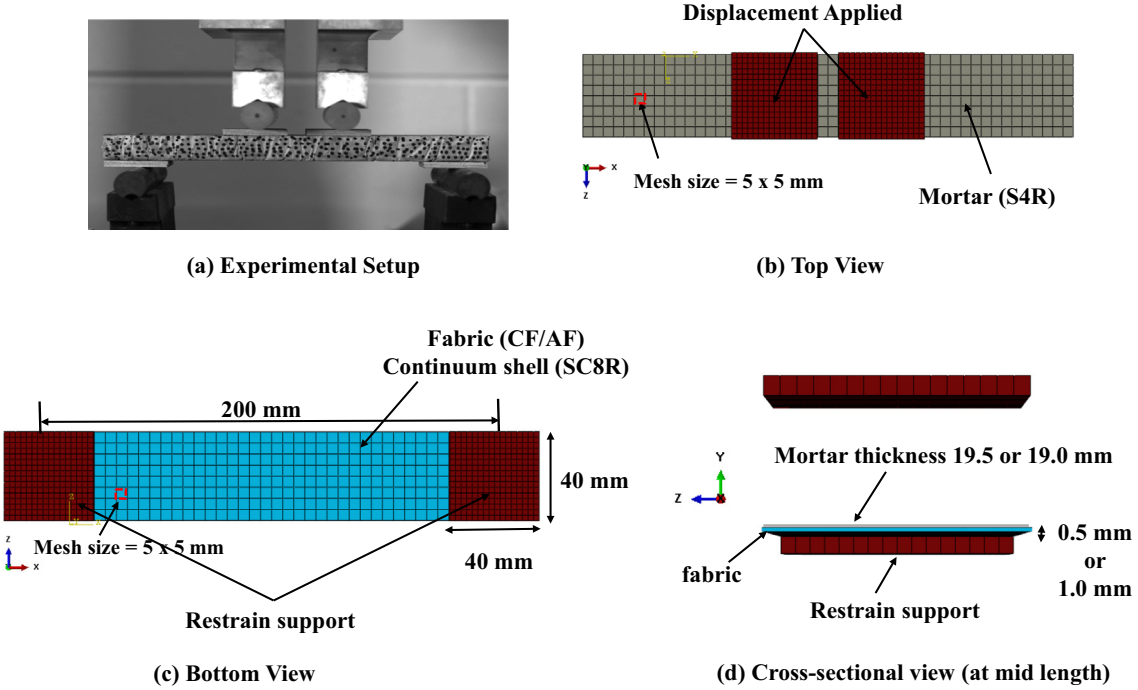

Fig. 19. FE model of the CF and AF composites.

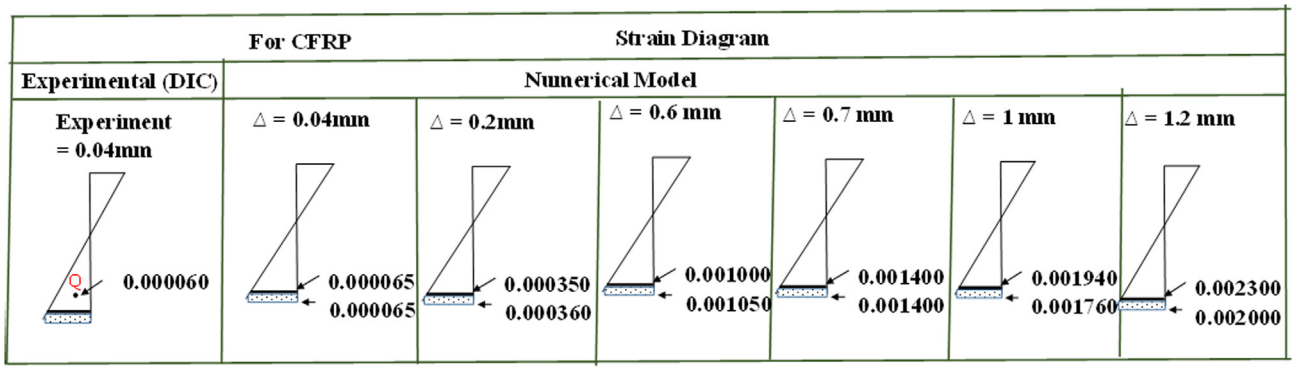

Fig. 20. Strain distribution in CF composite specimen: FE results.

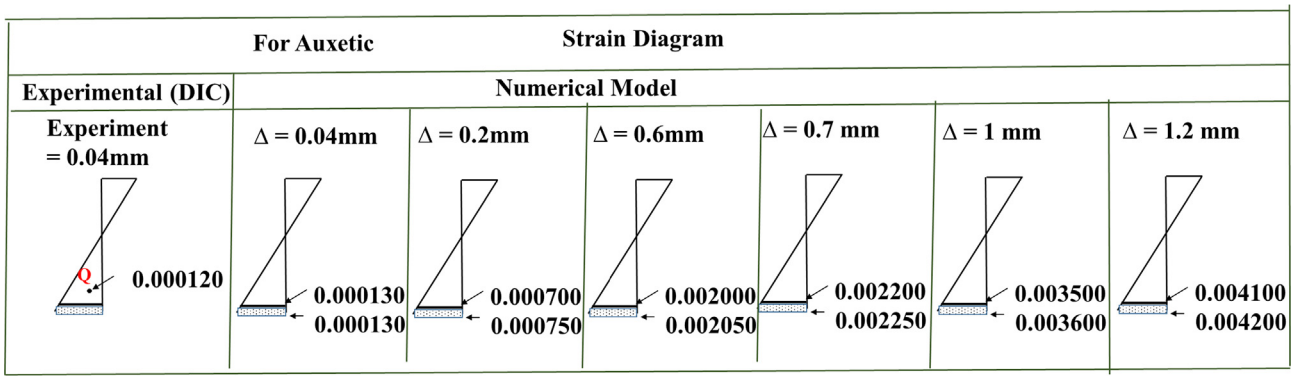

Fig. 21. Strain distribution in AF composite specimen: FE results.

ric became equal to the mortar strain and then remained lower than the mortar strain. From this observation, it can be inferred that the CF composite tend to delaminate from about 0.7 mm deflection level.

Whereas, as shown in Fig. 21, the AF fabric strain remained larger than that of the mortar (as it should be) for the whole of the analysis. Unlike the CF composite that exhibited delamination tendency beyond 0.7 mm deflection, the AF fabric continued to display strain larger than the mortar strain. Therefore, it is inferred that the AF fabric maintains its contact with the mortar as a true composite – reconfirming the experimental observation: the beneficial effect of the auxetic properties of the fabric overlayed with the polymer cement matrix. A similar model was also established for the inserted type specimens, the results of which matched with the overlay results presented here.

As the elastic FE model could not provide a comparison with the ultimate loads obtained from the experiments, theoretical calculations were performed at the ultimate stage defined as crushing localisation of the mortar matrix in Section 3.2 of this paper. For this purpose, the stress-strain characteristics of the cementitious polymer have been adopted from Zahra and Dhanasekar [11] – a replot of the data along with the idealised stress-strain relation is shown in Fig. 22. The idealised curve was used for the compression stress-block in the stress diagram for the calculation of the ultimate load as shown in Fig. 23.

It should be noted that for this simplified calculation, strain in the CF and AF were readout corresponding to the deflections of 4 mm and 13 mm respectively (described in Fig. 14(a) and (b) in Section 3.2 of the paper). At ultimate, the strain in the CF fabric was low due to delamination (52 μm) whilst the AF exhibited a strain of 30,000 μm. These strains were converted as stress in the

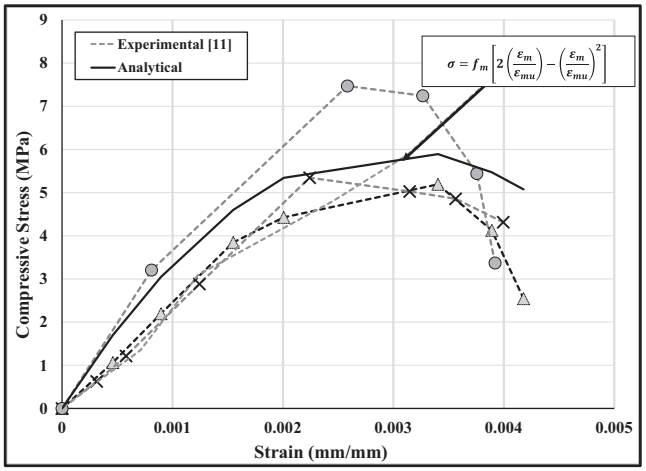

Fig. 22. Idealised stress-strain relation of cementitious matrix (mortar).

CF and AF fabrics using their respective stress-strain relations shown in Figs. 24 and 25.

Equating compression under the stress block above the neutral axis to the tension in the fabric (Eq. (1)), the equilibrium of forces were established.

$$C = \left(\int_0^{d_n} \sigma(y)dy = \zeta b f_m d_n^2\left[\frac{1}{\varepsilon_{mu}} - \frac{\zeta d_n}{3\,\varepsilon_{mu}{}^2}\right]\right) = T\left(= E_{fabric} \times \varepsilon_{fabric} \times A_{fabric}\right) \quad (1)$$

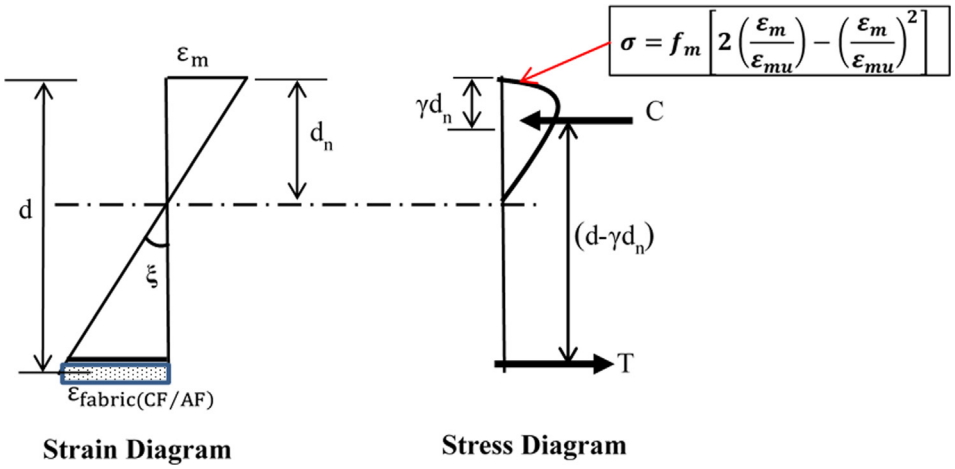

Fig. 23. Strain, stress and force diagrams for calculation of ultimate load.

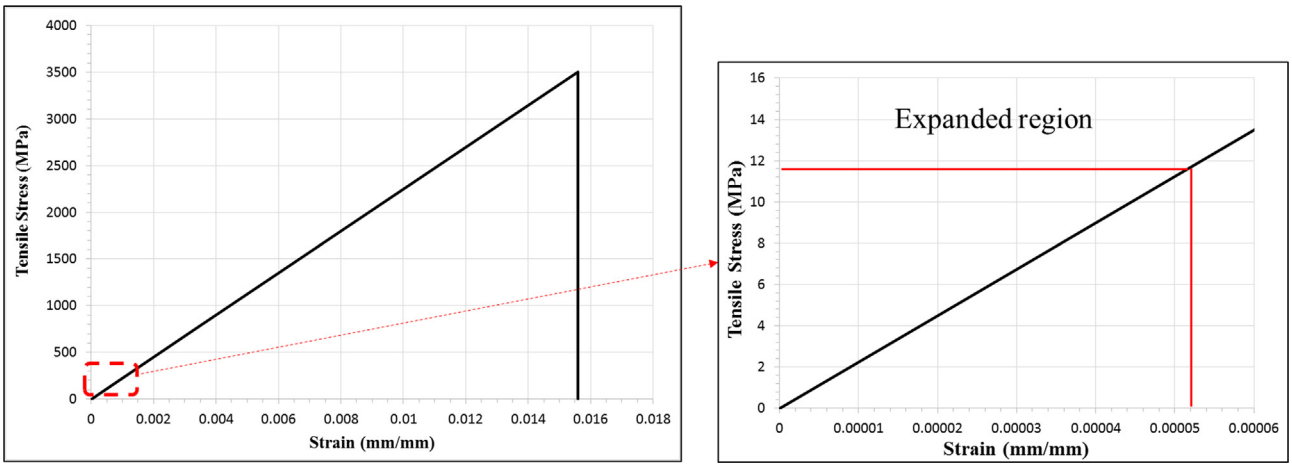

Fig. 24. Stress – strain diagram for CF fabric.

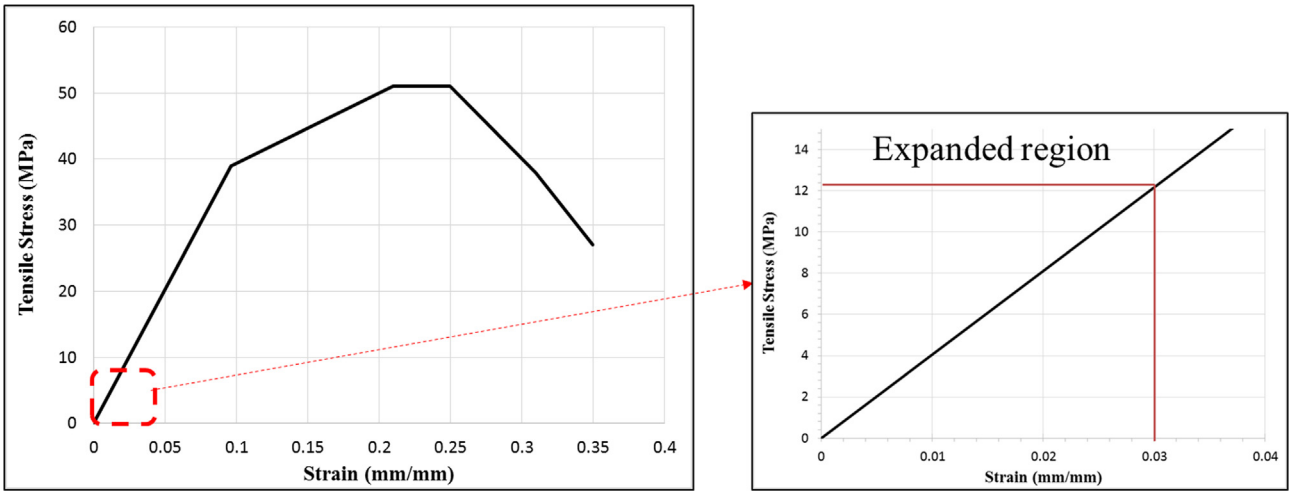

Fig. 25. Stress – strain diagram for AF fabric.

where,

$$f_m : \textit{compressive strength of mortar};\ d_n : \textit{depth of neutral axis};$$
$$\varepsilon_m : \textit{compression strain in mortar at extreme top};\ \varepsilon_{mu} : \textit{ultimate strain};$$
$$b : \textit{width of specimen};\ \zeta : \frac{\varepsilon_{fabric}}{d-d_n}$$

The ultimate moment was determined by multiplying the tension force in the fabric with the lever arm $(d-\gamma d_n)$, where

$$\gamma = 1 - \frac{\int_0^{\varepsilon_0} \varepsilon_m f_m d(\varepsilon_m)}{\varepsilon_0 \int_0^{\varepsilon_0} f_m d(\varepsilon_m)} \quad , \varepsilon_0 = \textit{strain at peak stress in compression} \tag{2}$$

The ultimate moment in CF and AF composites were determined as 3895 N mm and 8313 N mm respectively. The corresponding ultimate loads were 104 N and 222 N respectively that compared favourably with 105 N and 238 N determined experimentally.

5. Conclusions

This paper has presented an experimental investigation carried out to examine the methods of improving the energy dissipation characteristics of the polymer cement render. Carbon fibre (CF) and auxetic (AF) fabric inserts were used in the characterisation – overlayed and inserted configurations were explored. The investigation was carried out at four rates of loading, viz., 1, 50, 100 and 150 mm/min using four-point bending test specimens. The failure mode, peak load, load-displacement behaviour, debonding, longitudinal strain variation, and energy dissipation were studied from the test data of 72 specimens. An elastic finite element model with contact nonlinearity between the mortar matrix and the fabric was established to illustrate the differences in the CF and AF composites in terms of delamination. The following conclusions have emerged from the study:

- Auxetic fabric in the composite significantly improves the debonding and energy dissipation characteristics of the polymer-cement matrix. The best place to position the AF is close to the surface. The superior performance of AF inserted polymer-cement composite is attributed to its negative Poisson's ratio.
- AF composite has consistently exhibited improved response of peak load, longitudinal strain, energy dissipation with the increase in rate of loading. The energy dissipated by the AF specimens is about 134 times higher than that of controlled specimens at 1 mm/min loading rate that increases to 164 times of controlled specimens.
- AF has not increased the peak load of the polymer cement mortar matrix appreciably compared to the CF.
- AF inserts showed 2.6 times higher residual flexural strength than the CF composite at a loading rate of 150 mm/min.
- CF overlays/ inserts exhibited debonding and fibre fracturing. Although it provided significant contribution to the peak load, its energy dissipation was rather low (decreased by 25%) compared to AF polymer cement matrix composite.
- With the increase in the rate of loading (1–150 mm/min), the maximum longitudinal strain in the CF specimens lowered by 3.2 times than that of AF specimens.

The overlayed/ inserted AF – polymer cement matrix composites could be potentially used as a low-cost impact resistance rendering material for a buildings and wall structures.

The experiments considered only unidirectional fabrics (CF and AF); bi-directional fabrics might provide different characteristics and is worth examining.

Acknowledgements

The authors gratefully acknowledge the scholarship support and the tuition award from Queensland University of Technology (QUT), Australia. The involvement of Matthew Maroney and Benjamin Timms – two recent graduates in civil engineering, and Benjamin Brownlee, Senior Technician is thankfully appreciated.

References

[1] J.A. Barros, A. Fortes, Flexural strengthening of concrete beams with CFRP laminates bonded into slits, Cem. Concr. Compos. 27 (2005) 471–480.
[2] R. Capozucca, Static and dynamic response of damaged RC beams strengthened with NSM CFRP rods, Compos. Struct. 91 (2009) 237–248.
[3] M. Ferozkhan, R. Dhanasekar, W. Holt, M. Dhanasekar, Behaviour of Drystack Masonry Wallettes Under Axial Compression, in: 13th International Brick and Block Masonry Conference, Amsterdam, 2004, pp. 35–44.
[4] S. Pichandi, S. Rana, D. Oliveira, R. Fangueiro, Fibrous and composite materials for blast protection of structural elements—a state-of-the-art review, J. Reinf. Plast. Compos. 32 (2013) 1477–1500.
[5] Z.K. Awad, T. Aravinthan, Y. Zhuge, F. Gonzalez, A review of optimization techniques used in the design of fibre composite structures for civil engineering applications, Mater. Des. 33 (2012) 534–544.
[6] H. Gu, Z. Zhonge, Compressive behaviour of concrete cylinders reinforced by glass and polyester filaments, Mater. Des. 26 (2005) 450–453.
[7] M. Arduini, A. Nanni, Behavior of precracked RC beams strengthened with carbon FRP sheets, J. Compos. Constr. 1 (1997) 63–70.
[8] J. Teng, G. Chen, J. Chen, O. Rosenboom, L. Lam, Behavior of RC beams shear strengthened with bonded or unbonded FRP wraps, J. Compos. Constr. 13 (2009) 394–404.
[9] L. Ascione, V. Berardi, L. Feo, G. Mancusi, A numerical evaluation of the interlaminar stress state in externally FRP plated RC beams, Compos. B Eng. 36 (2005) 83–90.
[10] P. Buchan, J. Chen, Blast resistance of FRP composites and polymer strengthened concrete and masonry structures – a state-of-the-art review, Compos. B Eng. 38 (2007) 509–522.
[11] T. Zahra, M. Dhanasekar, Characterisation of cementitious polymer mortar–Auxetic foam composites, Constr. Build. Mater. 147 (2017) 143–159.
[12] M. Uzun, Mechanical properties of auxetic and conventional polypropylene random short fibre reinforced composites, Fibres & Textiles in Eastern Europe, 2012.
[13] P. Subramani, S. Rana, D.V. Oliveira, R. Fangueiro, J. Xavier, Development of novel auxetic structures based on braided composites, Mater. Des. 61 (2014) 286–295.
[14] X. Ren, R. Das, P. Tran, T.D. Ngo, Y.M. Xie, Auxetic metamaterials and structures: a review, Smart Mater. Struct. 27 (2018) 023001.
[15] S. Rana, R. Fangueiro, Advanced composites in aerospace engineering, Elsevier, Advanced Composite Materials for Aerospace Engineering, 2016, pp. 1–15.
[16] G. Imbalzano, P. Tran, T.D. Ngo, P.V. Lee, Three-dimensional modelling of auxetic sandwich panels for localised impact resistance, J. Sandwich Struct. Mater. 19 (2017) 291–316.
[17] M. Asad, M. Dhanasekar, T. Zahra, D. Thambiratnam, Mitigating impact failure of masonry boundary walls using auxetic composites, in: Proceedings of the 10th Australasian Masonry Conference, The University of Newcastle, Sydney, NSW, 2018, pp. 523–34.
[18] M. Assidi, J.-F. Ganghoffer, Composites with auxetic inclusions showing both an auxetic behavior and enhancement of their mechanical properties, Compos. Struct. 94 (2012) 2373–2382.
[19] M. Dhanasekar, T. Zahra, A. Jelvehpour, S. Noor-E-Khuda, D.P. Thambiratnam, Modelling of auxetic foam embedded brittle materials and structures, Appl. Mech. Mater. 846 (2016) 151.
[20] M. Dhanasekar, D. Thambiratnam, T.H. Chan, S. Noor-E-Khuda, T. Zahra, Modelling of masonry walls rendered with auxetic foam layers against vehicular impacts, in: 16th International Brick and Block Masonry Conference, Padova, Italy, 2016.
[21] N. Novak, M. Vesenjak, Z. Ren, Auxetic cellular materials – a review, J. Mech. Eng. 62(2016)9;485–493.
[22] K.E. Evans, M.A. Nkansah, I.J. Hutchinson, S.C. Rogers, Molecular network design, Nature 353 (1991) 124.
[23] W. Miller, Z. Ren, C. Smith, K. Evans, A negative Poisson's ratio carbon fibre composite using a negative Poisson's ratio yarn reinforcement, Compos. Sci. Technol. 72 (2012) 761–766.
[24] T. Zahra, M. Dhanasekar, Characterisation and strategies for mitigation of the contact surface unevenness in dry-stack masonry, Constr. Build. Mater. 169 (2018) 612–628.
[25] H. Davies, EN 1504: The European Standard for Concrete Repair, in: Proceeding of the Second RILEM/CISRO/ACRA International Conference on Rehabilitation of Structures, 1998. p. 600–7.

[26] J.A. Thamboo, M. Dhanasekar, Behaviour of thin layer mortared concrete masonry under combined shear and compression, Aust. J. Struct. Eng. 17 (2016) 39–52.
[27] J.A. Thamboo, M. Dhanasekar, C. Yan, Flexural and shear bond characteristics of thin layer polymer cement mortared concrete masonry, Constr. Build. Mater. 46 (2013) 104–113.
[28] J.A. Thamboo, M. Dhanasekar, Characterisation of thin layer polymer cement mortared concrete masonry bond, Constr. Build. Mater. 82 (2015) 71–80.
[29] M. Sloan, J. Wright, K. Evans, The helical auxetic yarn–a novel structure for composites and textiles; geometry, manufacture and mechanical properties, Mech. Mater. 43 (2011) 476–486.
[30] Nezamian A, Setunge S. Case study of application of FRP composites in strengthening the reinforced concrete. Headstock of a Bridge Structure, 2007.
[31] J.A. Thamboo, M. Dhanasekar, C. Yan, Effects of joint thickness, adhesion and web shells to the face shell bedded concrete masonry loaded in compression, Aust. J. Struct. Eng. 14 (2013) 291–302.
[32] S. Nazir, M. Dhanasekar, A non-linear interface element model for thin layer high adhesive mortared masonry, Comput. Struct. 144 (2014) 23–39.
[33] S. Nazir, M. Dhanasekar, Modelling the failure of thin layered mortar joints in masonry, Eng. Struct. 49 (2013) 615–627.
[34] F.I. Baratta, Requirements for flexure testing of brittle materials, Methods for Assessing the Structural Reliability of Brittle Materials: ASTM International, 1984.
[35] P. Frankovský, I. Virgala, P. Hudák, J. Kostka, The use the of digital image correlation in a strain analysis, Int. J. Appl. Mech. Eng. 18 (2013) 1283–1292.
[36] C. Barris, L. Torres, I. Vilanova, C. Miàs, M. Llorens, Experimental study on crack width and crack spacing for glass-FRP reinforced concrete beams, Eng. Struct. 131 (2017) 231–242.
[37] B. Pan, K. Qian, H. Xie, A. Asundi, Two-dimensional digital image correlation for in-plane displacement and strain measurement: a review, Meas. Sci. Technol. 20 (2009) 062001.
[38] S. Noor-E-Khuda, M. Dhanasekar, D.P. Thambiratnam, Out-of-plane deformation and failure of masonry walls with various forms of reinforcement, Compos. Struct. 140 (2016) 262–277.
[39] S. Noor-E-Khuda, M. Dhanasekar, Masonry walls under combined in-plane and out-of-plane loadings, J. Struct. Eng. 144 (2017) 04017186.
[40] S. Noor-E-Khuda, M. Dhanasekar, Three sides supported unreinforced masonry walls under multi-directional loading, Constr. Build. Mater. 188 (2018) 1207–1220.
[41] A. Naaman, S. Jeong, Structural ductility of concrete beams prestressed with FRP tendons, Non-metallic (FRP) reinforcement for concrete structures: proceedings of the second international RILEM symposium, CRC Press, 2004, p. 379.
[42] M.N. Hadi, J.S. Yuan, Experimental investigation of composite beams reinforced with GFRP I-beam and steel bars, Constr. Build. Mater. 144 (2017) 462–474.
[43] W. Rasband, ImageJ, US National Institutes of Health, Bethesda, MD, USA, 1997.
[44] S. Noor-E-Khuda, M. Dhanasekar, D.P. Thambiratnam, An explicit finite element modelling method for masonry walls under out-of-plane loading, Eng. Struct. 113 (2016) 103–120.
[45] A.W. Page, P.W. Kleeman, M. Dhanasekar, An in-plane finite element model for brick masonry, New Analysis Techniques for Structural Masonry: ASCE, 1985, p. 1–18.
[46] M. Dhanasekar, W. Haider, Explicit finite element analysis of lightly reinforced masonry shear walls, Comput. Struct. 86 (2008) 15–26.